RESONANT MODE INTERACTION IN A CANONICAL SEPARATED FLOW

Rajat Mittal and Rupesh B. Kotapati
Department of Mechanical and Aerospace Engineering, The George Washington University Washington DC 20052, USA

(*Proceedings of the IUTAM Symposium on Laminar-Turbulent Transition, December 2004, Bangalore, India.*)

1. Introduction

The current study is directed towards understanding the flow physics of separated flows over airfoils with the ultimate goal of developing effective zero-net-mass-flux (ZNMF) jet based active separation control (ASC) strategies. The key control parameters in a ZNMF device are the jet frequency f and jet velocity V_J . The former is usually non-dimensionalized as $F^+ = f/f_n$ where f_n is some natural frequency in the uncontrolled flow. The latter is non-dimensionalized by U_∞ . Note that V_J is some characteristic measure of the jet velocity, such as the peak or an average velocity. As expected, control authority varies monotonically with V_J/U_∞ (Seifert *et al.* 1996, Glezer & Amitay 2002; Mittal & Rampunggoon 2002) up to a point where a further increase would likely completely disrupt the boundary layer. Thus, there is little possibility of extracting an "optimal" value of this parameter. On the other hand, control authority has a highly non-monotonic variation with F^+ (Seifert & Pack 2000; Glezer et al. 2003) and this not only suggests the presence of rich flow physics and multiple flow mechanisms but also reveals the potential of optimizing the actuation scheme with respect to this parameter.

Current strategies for ZNMF based separation control are explicitly or implicitly based on the proposition that the dynamics of a separated flow over an airfoil are dominated by the characteristic frequency of the separation region, f_{sep} and that $f_{sep} \sim U_\infty/L_{sep}$ where L_{sep} is the length of the separation region. However the situation is significantly more complex than this. Based on past studies (Chang 1976, Wu et al. 1998), one can consider the following three situations for flow past an airfoil. Case A represents attached flow at low angle-of-attack (AOA) where the boundary layer on the suction side develops under an adverse pressure gradient but does not separate. Such a flow

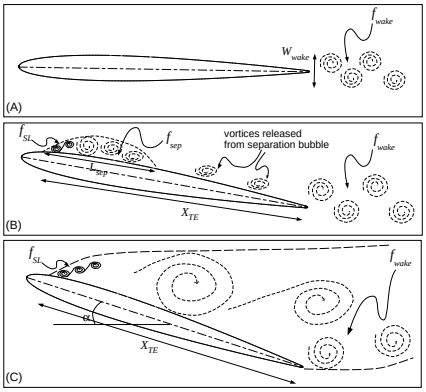

Figure 1. Three different scenarios for flow past an airfoil.

has one dominant wake shedding frequency f_{wake} which, according to Roshko (1954) scales as U_∞/W_{wake} . In direct contrast to Case A is the situation at high AOA, namely the post-stall Case C where separation occurs near the leading-edge and the flow does not reattach (in the mean) to the airfoil surface. This flow behaves like that past a bluff body and is consequently subject to two frequency scales, f_{SL} and f_{wake}, where the former is the natural vortex rollup frequency of the shear layer and the latter is again the frequency corresponding to vortex shedding in the wake. Finally, Case B corresponds to the situation where separation occurs at some location downstream of the leading edge, and the separated shear layer may or may not reattach before the trailing edge (Chang 1976). If the flow reattaches before the trailing edge, there are potentially three frequency-scales: f_{SL} , f_{wake}, and f_{sep}, the frequency scale corresponding to the separation "bubble." It is quite clear that the nonlinear interactions between these various flow features will drive the temporal dynamics and transition process for this flow. This also has implications for ZNMF based separation control since it clearly indicates that f_{sep} is just one of the three naturally occurring frequencies in a separated airfoil and an effective separation control strategy should take account of these multiple frequencies and associated mechanisms.

However, our understanding of the dynamics of this resonant mode interaction is somewhat limited. Past approaches to studying these issues have mostly employed conventional airfoil geometries where the flow separation is produced by varying angle-of-attack and/or freestream velocity. Although this approach is obviously grounded in practical reality, it is not the best one for a precise investigation and delineation of the various physical mechanisms that are potentially implicated in ASC. Thus, a configuration is needed that (1) is simple and includes all the important features of a canonical separated airfoil

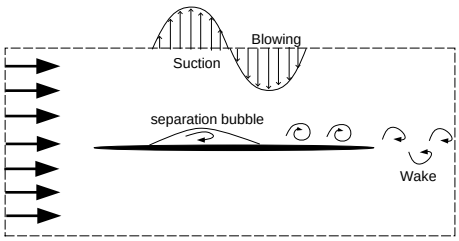

Figure 2. Schematic of canonical separated flow configuration used in current study

flow, including leading edge boundary layer inception, suction side separation (open as well as closed separation), (2) has a wake which includes vortices from the suction and pressure sides; and (3) allows independent prescription of the location and extent of the separation region as well as the Reynolds number. A novel configuration that satisfies these criteria has been devised and is described below.

2. Flow Configuration

The configuration to be studied involves a thin flat-plate (chord length c and thickness t) as shown in Fig. 2. Separation is induced on the upper surface of this plate by applying blowing and suction on the upper boundary of the computational domain as shown in the schematic. The technique of Na & Moin (1998) will be adopted wherein the following boundary condition is prescribed on the upper wall

$$u_y = G(x); \qquad \frac{\partial u_x}{\partial y} = \frac{dG}{dx}; \qquad u_z = 0, \tag{1}$$

where $G(x)$ is the prescribed blowing and suction velocity profile, and the boundary condition on u_x ensures that no spanwise vorticity is produced due to the blowing and suction. The key aspect of this approach is that the function $G(x)$ allows us to prescribe the streamwise L_{sep} and cross stream size H_s of the separation region as well as its location. Thus, separation can be produced anywhere on the plate surface and can therefore reproduce any of the three separated flow situations discussed in the previous section. The above configuration can be employed to examine the nonlinear interactions between the shear layer, separation region, and airfoil wake in uncontrolled and ZNMF-based controlled versions of these flows. Note that the confounding effect of curvature is absent here, something that is not usually possible with conventional airfoil investigations.

3. Numerical Method

A finite-difference based approach for computing flows with moving immersed solid three-dimensional boundaries on fixed Cartesian grid has been developed. The key feature of this method is that simulations with complex boundaries can be carried out on stationary non-body conformal Cartesian grids and this eliminates the need for complicated remeshing algorithms that are usually employed with conventional Lagrangian body-conformal methods.

The governing equations are the incompressible Navier-Stokes equations which are discretized using a cell-centered, collocated (non- staggered) arrangement of the primitive variables. The equations are integrated in time using the fractional step method. In the first step, the momentum equations without the pressure gradient terms are first advanced in time. In the second step, the pressure field is computed by solving a Poisson equation. A second-order Adams-Bashforth scheme is employed for the convective terms while the diffusion terms are discretized using an implicit Crank-Nicolson scheme, which eliminates the viscous stability constraint. The solution of pressure Poisson equation (PPE) is the most time consuming part of the solution algorithm. In the current solver an efficient multigrid methodology has been developed which is well suited for use in conjunction with the immersed boundary method. A compressible version of the solver is described in Ghias *et al*. (2004).

4. Results and Discussion

Two-dimensional simulations of this configuration using a 2% thick elliptic airfoil at a chord Reynolds number of 60,000 have been carried out. These serve to demonstrate the validity of the proposed approach as well as the numerical capabilities of the immersed boundary solver employed. All simulations reported here have been carried out on a single processor, 2.4 MHz, Pentium-4 workstation. Fig. 3a shows the spanwise vorticity contour plot for the baseline unseparated flow and the plot shows the presence of Karman vortex shedding in the wake. Fig. 3b shows the temporal variation of cross-stream velocity component at $x/c = 0.25$ (top), 0.5 (middle) and 1.25 (bottom) where x is measured from the leading edge, and it can be seen that even far upstream of the trailing edge, the global signature of the wake vortex shedding is present. The frequency of vortex shedding, when normalized with the momentum thickness of the wake and the freestream velocity, gives a value of roughly 0.14 which is consistent with the scaling of Roshko (1954).

This baseline case is subsequently subjected to sinusoidal blowing and suction on the top boundary to induce separation. Two different cases are simulated. The first one is of a closed mid-chord separation where the blowing and suction extends from $x/c = 0.25$ to 0.75 and the second one is a

case of trailing-edge separation where the blowing and suction extends from $x/c = 0.50$ to 1.0. Fig. 4 shows pressure along a horizontal line above the top surface of the airfoil with adverse pressure gradient induced by blowing-suction on top boundary at two different locations. Examination of the mean flow shows that in the first case, a recirculation bubble of length $L_{sep} \approx 0.3c$ is created whereas in the second the bubble length is $0.35c$.

Fig. 5a shows a sequence of spanwise vorticity contour plots that show a flow rich in distinct vertical interactions. First, the boundary layer is seen to separate at the location where the suction become active ($x/c = 0.25$) and this separated shear layer immediately starts rolling up into small scale Kelvin-Helmholtz type vortices. Some of these vortices are seen to merge and form larger vortices and this leads to the formation of larger vortices in the separation region. At periodic intervals, one of these large vortices is released from the separation bubble and it travels downstream where it intermittently disrupts the Karman vortex shedding in the wake. Thus, this one example clearly shows all of the features that we have claimed will be present on a canonical separated flow. Examination of temporal variation of flow variable allows us to extract the three distinct frequencies. Fig. 5b shows the variation of cross-stream velocity component at the separation point ($x/c = 0.25$), at the center of the separation bubble ($x/c = 0.50$) and in the wake at ($x/c = 1.25$). The first and second plots clearly show the presence of the high shear layer frequency as well as the lower separation bubble frequency which corresponds to the release of the vortex by the separation bubble. The third plot also clearly shows how the high frequency vortex shedding is disrupted periodically by the separation vortex. For this case, $f_{sep}L_{sep}/U_\infty$ is about 0.42. Furthermore, the shear layer frequency f_{SL} is about $7f_{sep}$ whereas the vortex shedding f_{wake} frequency is about $19f_{sep}$.

Fig. 6a shows a sequence of spanwise vorticity contour plots for the second case and comparison with previous case illustrates the potential effect of separation bubble location on the flow. Overall the interaction between the three features of the flow (shear layer, separation bubble and wake) are qualitatively similar to that seen in the previous case. For this case, $f_{sep}L_{sep}/U_\infty$ is about 0.19 which is quite low and this is likely due to the effect of the wake on the separation dynamics. This underscores our earlier conjecture that $f_{sep}L_{sep}/U_\infty$ can be significantly different from unity depending on the flow configuration. The flow is clearly more chaotic than the previous case and this is likely due to the interaction between the separation region and wake instabilities. Interestingly however, shear layer frequency f_{SL} is about $6f_{sep}$ which is similar to the previous case and the vortex shedding frequency f_{wake} is about $19f_{sep}$ which matches the previous case also. Therefore, there is some indication that the shear layer and wake seem to "lock-on" to the separation region frequency which itself seems to be modified by virtue of being in the

vicinity of the wake. This again provides some validation to the resonant-mode interaction that we have hypothesized is important in such flows.

Acknowledgments

This research is supported by grants from NASA and AFOSR.

References

Chang, P. K., Control of Separation, McGraw-Hill, New York, 1976.

Glezer, A. and Amitay, M., "Synthetic Jets," *Ann. Rev. Fluid Mech.*, 34:503-29, 2002.

Ghias, R., Mittal, R., and Lund, T., S., "A Non-Body Conformal Grid Method for Simulation of Compressible Flows with Complex Immersed Boundaries," AIAA Aerospace Sciences Meeting, 2004.

Glezer, A., Amitay, M., and Homohan A. M., "Aspects of Low- and High-Frequency Aerodynamic Flow Control," AIAA-2003-0533, 2003.

Mittal, R. and Rampunggoon, P., "On the Virtual Aero-Shaping Effect of Synthetic Jets," *Phys. Fluids*, vol. 14, no. 4., pp. 1533-1536, 2002.

Roshko, A. "On the Development of Turbulent Wakes from Vortex Streets," NACA Report 1191, 1954.

Na, Y. and Moin, P., "Direct Numerical Simulation of a Separated Turbulent Boundary Layer," *J. Fluid Mech.*, vol. 370, pp. 175-201, 1998.

Seifert, A., Darabi, A. and Wygnanski, I., "Delay of Airfoil Stall by Periodic Excitation," *J. Aircraft*, vol. 33, pp. 691-698, 1996.

Seifert, A. and Pack, L. G., "Oscillatory Control of Separation at High Reynolds Numbers," *AIAA J.*, vol. 37, no. 9, pp. 1062-1071, Sep. 1999

Wu, J. -Z., Lu, X. -Y., Denny, A. G., Fan, M., and Wu, J. -M. "Post-Stall Flow Control on an Airfoil by Local Unsteady Forcing," *J. Fluid Mech.*, vol. 371, pp. 21-58, 1998.

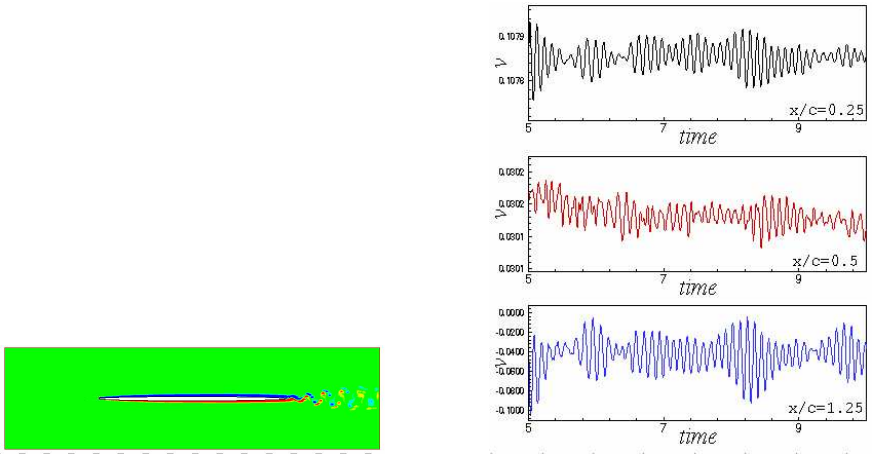

(a) (b)

Figure 3. Spanwise vorticity contour plot and temporal variation of cross-stream velocity at three locations for baseline case with no induced separation.

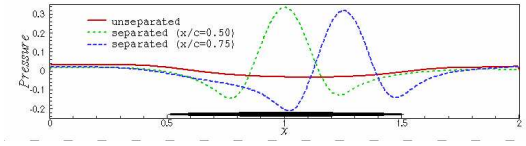

Figure 4. Variation of pressure in the streamwise direction above the top surface of the airfoil.

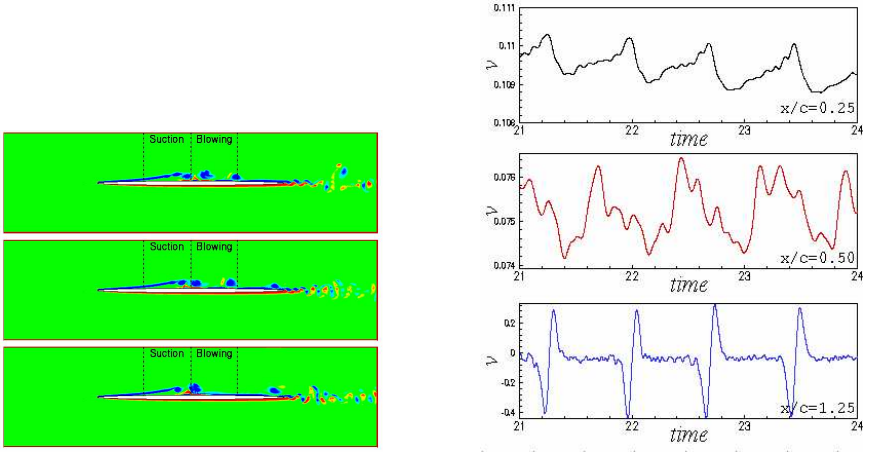

(a) (b)

Figure 5. Sequence of spanwise vorticity contour plots and temporal variation of cross-stream velocity at three locations with separation induced at the mid-chord.

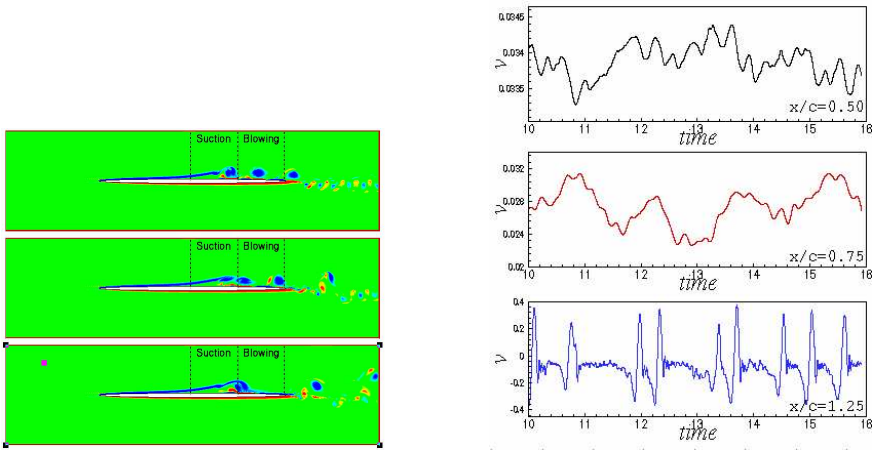

(a) (b)

Figure 6. Sequence of spanwise vorticity contour plots and temporal variation of cross-stream velocity at three locations for with separation induced on the aft half of the airfoil.